Towards a Realistic MISO Simulation: Impact of Rectification

Maheswar Pradhan
Indian Institute of Technology Bombay
Suryachandra A. Rao (surya@tropmet.res.in)
Ministry of Earth Sciences
Amitabh Bhattacharya
Indian Institute of Technology

Research Article

Keywords:

Posted Date: January 27th, 2023

DOI: https://doi.org/10.21203/rs.3.rs-2506933/v1

Additional Declarations: No competing interests reported.

Version of Record: A version of this preprint was published at Climate Dynamics on January 8th, 2024.
See the published version at https://doi.org/10.1007/s00382-023-07053-6.

Abstract

State-of-the-art coupled models have several limitations in representing the phase and amplitude characteristics of monsoon intra-seasonal oscillations (MISO). Specifically, the models' deficiencies in predicting stronger active spells have been widely reported in earlier studies. In the present study, we endeavour to overcome this limitation by better representing the diurnal cycle of the sea surface temperature and the associated feedback processes. In the present study, we demonstrate that resolving the diurnal cycle rectification in a state-of-the-art global coupled model improves the simulation of MISO. The present analysis showcases how rectification can modulate the oceanic, atmospheric and interfacial properties so that the coupled model can better simulate stronger active monsoon spells. The essential requirements for the coherent northward propagation mechanism of MISOs are pronounced in the presence of intra-seasonal rectification by diurnal SSTs.

1. Introduction

Monsoon intra-seasonal oscillations (MISO) are one of the prominent features during boreal summer in the Indian monsoon region. MISOs are the periodic oscillation of dry (break) and wet (active) spells of precipitation which have a time scale longer than diurnal and synoptic variability but shorter than a season. Earlier studies (ALEXANDER et al. 1978; Yasunari 1980; Goswami and Ajaya Mohan 2001) have shown that MISOs have a preferred scale of periodicity between 20 to 90 days. A repeated northward movement of cloud bands from south of the equator to the foothills of the Himalayas is associated with active and break spells of monsoon (Yasunari 1979; Sikka and Gadgil 1980; Krishnamurti and Subrahmanyam 1982). The frequency, length, and intensity of active and break spells can also modulate the seasonal mean rainfall during a calendar year (Goswami and Ajaya Mohan, 2001). Accurate prediction of MISO phase and amplitude is critical for planning activities like agriculture, water availability, and power supply (Gadgil and Rupa Kumar; Prasanna 2014; Dunning et al. 2015; Roy et al. 2022), etc.

Earlier studies have suggested several mechanisms for the northward propagation of MISOs (Webster 1983; Goswami and Shukla 1984; Wang and Xie 1997; Kemball-Cook and Wang 2001; Jiang et al. 2004). Based on results from observation and a simple general circulation model, Jiang et al. (2004) proposed two mechanisms for the northward propagation of convection bands: (a) vertical wind shear mechanism and (b) moisture-convection feedback mechanism. The vertical wind shear mechanism is effective away from the equator, and moisture-convection feedback is responsible for propagation near the equator. The vertical wind shear mechanism generates barotropic positive (negative) vorticity on the northern (southern) front of the convection center as a result of interaction between vertical shear on easterly flow and meridional gradient of the baroclinic divergence. The barotropic vorticity further leads to the development of barotropic divergence in the free atmosphere north of the convection centre. The free atmosphere divergence results in a boundary layer convergence, and convective heating moves north of the previous convection center. The second mechanism responsible for the northward propagation of

MISO is via moisture convergence by intra-seasonal winds north of the convection center in the presence of meridional asymmetry of specific humidity.

The air-sea interaction is another physical aspect that governs the life cycle of MISOs (Krishnamurti *et al.*, 1988; Sengupta *et al.*, 2001; Vecchi and Harrison, 2002). In this mechanism, due to the calm wind conditions, the latent surface heat is decreased (and net heat flux into the ocean increased), resulting in positive sea surface temperature (SST) anomalies to the north of the convection center. As a result, the moisture convergence is enhanced, destabilizing the lower atmosphere (Roxy et al. 2013) north of the convection center, and the convection center moves further northward. The ineludible role of the ocean on MISO dynamics (Webster et al. 1998; Ajayamohan et al. 2008) and better simulation of MISO phase and amplitude using coupled models (rather than standalone models) are being progressively recognized (Kemball-Cook and Wang 2001; Wu et al. 2002; Fu et al. 2003; Seo et al. 2007; Sabeerali et al. 2013; Sharmila et al. 2013; Li et al. 2018). Although most of the coupled models could capture the northward propagation of MISOs satisfactorily, the models have limited capability for the coevolution of atmospheric convection and sea surface state (Goswami et al. 2014). The amplitude of active/break spells is underestimated, and the northward propagation of MISOs is slower in coupled models compared to the observation (Goswami et al. 2014; Li et al. 2018. Li et al. (2018) have analyzed Climate Forecast System version 2 (CFSv2) forecasts. They have found that the air-sea interaction is underrepresented over the Arabian Sea (AS) and Bay of Bengal (BoB) during intra-seasonal oscillations. The amplitude of MISO was found to be underestimated due to extremely weak response of SST to surface fluxes and convection to SST. They have suggested the inclusion of ocean skin layer and better resolving diurnal cycle as the ways to improve the MISO characteristics in coupled models. Based on their suggestion, the present study is designed to improve the simulation of MISO dynamics by implementing diurnal skin temperature parameterization in coupled models.

The surface ocean exhibits significant diurnal, seasonal, and inter-annual variability (Kawai and Wada 2007). Two processes that are responsible for diurnal skin temperature variability are: (a) daytime warming and (b) night-time cooling, and they are the result of intra-daily variability of mixed layer depth (MLD). The diurnal MLD and SST variability is widely reported by various observational and modelling studies (Pradhan et al. 2022 and the references therein). The upper ocean's diurnal mixing (and hence diurnal ocean temperature variations) is modulated by stabilizing effects of incident solar radiation and destabilizing effects of outward radiative fluxes (such as outgoing long wave radiation, latent and sensible heat) and wind-driven mixing. These atmospheric forcings (solar radiation, wind speed, cloud, or convection) have dominant intra-seasonal variability linked to the MISOs. Therefore, diurnal sea surface variability can be modulated by the intra-seasonal atmospheric variabilities (Bernie et al. 2005; Shinoda 2005; Bellenger and Duvel 2009; Thushara and Vinayachandran 2014; Yan et al. 2021). On the other hand, observational as well as modelling studies (Slingo et al. 2003; Dai and Trenberth 2004; Brunke et al. 2008; Bellenger et al. 2010; Masson et al. 2012; Clayson and Bogdanoff 2013; Reeves Eyre et al. 2021; Pradhan et al. 2022) have shown that the diurnal cycle of SST can modulate ocean and atmospheric fields at diurnal and longer time scales such as sub-seasonal, seasonal, interannual and climatological scales. Although a vast number of studies (Chen and Houze 1997; Slingo et al. 2003; Seo et al. 2014) can

be found on the role of diurnal warming on different phases of Madden Julian Oscillation (MJO another intra-seasonal oscillation over tropical latitudes, Madden and Julian 1971), limited studies are available on addressing the role of diurnal warming on the life cycle of intra-seasonal oscillations in monsoon domain. The present study follows up on the previous work by Pradhan et al. (2022), in which better representation of diurnal cycle of skin temperature was shown to be crucial in improving diurnal phase and amplitude of SST, MLD, fluxes and precipitation etc in CFSv2. The present study addresses whether the SST diurnal cycle has any role in the earlier proposed mechanisms by Jiang et al. (2004) and Kemball-Cook and Wang (2001) for northward propagating MISOs. The article is arranged as follows: section 2 discusses the observational data used and the choice and design of model experiments, section 3 discusses the results, and section 4 summarises the results from the analysis, respectively.

2. Data And Methodology

2.1. Coupled Model Experiments

Dynamical model sensitivity experiments are carried out using CFSv2 (Saha et al. 2014). A modified version of CFSv2 (Rao et al. 2019) is being used for operational seasonal and extended-range prediction at the India Meteorological Department (IMD), India. Earlier studies attempted to improve simulation of MISOs in CFSv2 by improving convective parameterization scheme (Ganai *et al.*, 2019), cloud micro physics (Dutta *et al.*, 2021), and representation of river-runoff variability (Srivastava et al. 2022; under review) etc. The present study explores another direction of improving MISO simulation using CFSv2 which is by implementing diurnal ocean skin temperature parameterization. Therefore, two hindcasts are generated using the CFSv2 model: (a) without diurnal parameterization for ocean skin temperature and (b) with a diurnal parameterization for ocean skin temperature. Therefore, in the first set of hindcast (termed as CTL run hereafter), the ocean bulk temperature. i.e., the temperature at 5m is considered SST. The bulk temperature acts as boundary forcings to the atmospheric component in the CTL run. The surface fluxes (latent heat, sensible heat, longwave radiation) are derived based on this temperature. On the other hand, in the second set of hindcast (termed as SEN hereafter), skin temperature computed using the algorithm developed by Fairall et al. (1996a) acts as boundary forcing to the atmospheric component. The diurnal skin temperature is derived from bulk ocean temperature by implementing cool skin and warm layer temperature corrections. The detailed formulation can be found in Fairall et al. (1996a) and also summarized in Pradhan et al. (2022). The CTL and SEN experiments also differ regarding the parameterization of turbulent surface fluxes, namely the latent heat, sensible heat, and wind stress. CTL simulations follow NCAR (National Center for Atmospheric Research) algorithm (Large and Yeager 2009) and SEN simulations follow COARE3.0 (Fairall et al. 1996b, 2003) for turbulent flux computation. The atmospheric component of the model has a horizontal spectral resolution of T126 (~100 Km), and the ocean model is a finite difference model with varying horizontal resolution (0.25° between 10°S to 10°N latitude band and gradually increasing to 0.5° near poles). The atmosphere model has a time step of 10 min, and the ocean model has a time step of 30 min, and they are coupled every 30 min of the model time step. The model output frequency is set to 3 hours for these simulations. The simulations are

computationally expensive (~ 800 CPU hours for 1 set of experiments); hence, the 3-hourly hindcasts are limited from 1998 to 2008. Wherever high-frequency (3 hourly) fields are not required, the analysis is extended from 1998-2017.

2.2. Observations/Reanalysis

The analyses in the present study are carried out to see the impact of the diurnal cycle on intra-seasonal oscillations and focus on boreal summer (June to September) unless stated explicitly. Satellite-derived SST data is taken from SeaFlux (Curry et al. 2004), available at a horizontal resolution of 0.25° and a temporal resolution of 1 hour. Tropical Rainfall Measuring Mission (TRMM; Huffman et al., 2010) precipitation data is considered for diurnal and intra-seasonal analysis and is available at 0.25° horizontal and 3-hour temporal resolution. Hourly/daily ocean sub-surface temperature data is obtained from tropical moored buoy observing systems: TAO/TRITON and RAMA at several Pacific and Indian Ocean locations. The moored buoy observations are used explicitly for model validation. Sensible heat and latent heat flux data are obtained daily from the Objectively Analyzed air-sea Fluxes (OAFlux; Yu et al. 2008) dataset and compared against SeaFlux and TropFlux(Kumar et al. 2011) dataset. The Japanese 55-year Reanalysis (JRA55; Kobayashi et al. 2015) dataset is considered from 1000hpa to 100 hPa level for column integrated moisture and moist static energy budget terms. JRA55 data set has a horizontal resolution of 1.25°.

3. Results

3.1. MISO characteristics

An intra-seasonal signal is first obtained by applying a 20–100-day Lancozs bandpass filter to daily rainfall anomalies. The MISO index is defined as the standardized filtered rainfall anomalies averaged over central India (15°N-25°N, 70°E-85°E). This selection covers the narrow-tilted belt extending from the northern BoB to the Western Ghats and eastern AS over which maximum intra-seasonal variability in precipitation lies. Active (cycles) are defined as days when the MISO index is greater (less) +1(-1). Hovmöller analysis of rainfall anomalies for most significant (coherent) northward propagating MISOs is also carried out during the active phase of monsoon. Coherent MISO events which propagate from the equator to 20°N and bear similar phase structures at a given latitude are determined following Jiang et al. (2004), Ajayamohan et al. (2008), and Sabeerali et al. (2014). The longitudinally (85°E-95°E) averaged filtered rainfall anomalies (colour shading) for the coherent MISOs over BoB during the active phase of the monsoon are plotted in Fig.1(a)-(c). In observation, positive anomalies start over the southern BoB at -20 days and propagate northward to +10 days. The subsequent break phase with negative rainfall anomalies starts at southern BoB around the 0th day and propagates northward to higher latitudes up to +20 day. During the active phase, stronger positive rainfall anomalies can be seen over 10°N-20°N latitude during -10 to +10 days. A similar active phase followed by a break phase in rainfall anomalies can be seen in CFSv2 CTL simulations. However, significant differences in terms of amplitude,

organization, and propagation of anomalies can be noted in the model. The propagation of MISO anomalies is slower in the model CTL simulation. The CTL simulated rainfall anomalies during the active phase of the monsoon are weaker in magnitude, specifically at higher latitudes. Li et al. (2018) reported rapid growth of errors in model-simulated MISO anomalies beyond 12°N. The problems mentioned above, related to MISO amplitude and propagation, are due to the errors in air-sea coupling in models as suggested by earlier studies (Wang et al. 2009; Sharmila et al. 2013; Srivastava et al. 2017; Li et al. 2018). Li et al. (2018) have also analyzed CFSv2 forecasts and have found that the air-sea interactions are underrepresented over the Arabian Sea and BoB during intra-seasonal oscillations. The amplitude of MISO was underestimated due to too weak SST response to surface fluxes and convection response to SST. They have suggested the inclusion of ocean skin layer and better resolving diurnal cycle as the ways to improve the MISO characteristics in coupled models. Therefore, this section addresses the impact of including diurnal skin temperature parameterization (SEN run) on simulating MISO amplitude and propagation characteristics. With the diurnal cycle of SST, stronger active and subsequent break phases are seen in the SEN compared to the CTL run. The positive rainfall anomalies during the active phase are stronger in SEN run from the equator to northern latitudes. Hovmöller analysis of rainfall anomalies centred around the peak break phase (figure not shown) shows that rainfall anomalies during both the break phase and the following active phase are significantly stronger, and they propagate to higher latitudes in SEN run (20°N) compared to CTL run (16°N). Therefore, in SEN simulations, the active phase after the break phase bears a better resemblance with the observed ones. The underlying mechanism for this difference in meridional propagation characteristics in the presence/absence of the SST diurnal cycle is further discussed.

3.2. MISO Mechanism

As discussed earlier, among various mechanisms proposed for poleward propagation of MISOs, "vertical wind shear" and "moisture-convection feedback" mechanisms postulated by Jiang et al. (2004) are widely accepted. These mechanisms examine the meridional relationship of various atmospheric fields linked to northward propagating MISOs. Meridional asymmetry in the vertical structure of circulation and convective parameters around the convection center are the prominent features supporting these mechanisms. Therefore, the vertical profiles of vertical velocity, specific humidity, vorticity, and divergence are composed at different latitudes with respect to the maximum convection center and are shown in Fig. 2. The vertical profiles are obtained by averaging over 80°E-95°E longitudes over BoB. The meridional structure of vertical velocity shows that maximum vertical motion is located at the convection center and occurs in the middle troposphere (around ~500 hPa). A northward shift of vertical motion at a lower level can be seen in Fig. 2(a), resulting in tilting the maximum vertical velocity axis. The northward shift of the maximum vertical velocity axis is extended up to 6° north of the convection center. The ascending motion is associated with a low-level convergence and upper-level divergence, as shown in Fig. 2(d). The maximum upper-level divergence is collocated with the convection center, whereas the maximum low-level convergence leads the convection center by a few degrees. In the specific humidity profile (Fig 2. g), the maxima lie around 700 hPa in the reanalysis. A poleward shift similar to vertical velocity is seen in the

axis of maximum specific humidity. The specific humidity profile tilts at lower levels up to 2° north of the convection center. The vorticity field shows a clear meridional asymmetric structure around the convention center. An equivalent barotropic positive vorticity is located north of the convection center, whereas similar equivalent barotropic negative vorticity is located south of the convection center. The positive barotropic vorticity is located 2° north of the convection center. A similar northward shift is also seen in the vertical profile of geopotential height (Supplementary 1). The meridional structure of the vertical profile of Moist static energy (MSE) resembles that of specific humidity with maxima located around 5° north of the convection center and tilting of maximum vertical MSE axis in the lower atmosphere (Supplementary 1). These observed features are similar to that of reported earlier studies with insignificant differences due to the different study periods and reanalysis dataset considered in this study. Based on these features, Jiang et al. (2004) proposed that during the active phase of MISO, a baroclinic divergent motion (i.e., upper-level divergence and lower-level convergence) with maximum vertical motion in the middle troposphere appears because of the convective heating in the middle troposphere. The interaction between this baroclinic divergence and a strong easterly shear in the monsoon regions results in a positive (negative) barotropic vorticity north (south) of the convection center. The positive barotropic vorticity further develops a free-atmosphere divergence north of the convection center. As a result, boundary layer convergence increases north of the convection center (due to Ekman pumping). The low-level moisture convergence shifts the center of convective heating to the north of the previous convection center. Therefore, dynamical features essential for coherent northward propagation of MISO can be summarised as (a) Meridional asymmetry in vertical profiles of vertical velocity, divergence, vorticity, specific humidity, and geopotential height. (b) northward shift of the axis of maximum at a lower level in various parameters such as vertical velocity, vorticity, specific humidity, geopotential height, and moist static energy (MSE; Supplementary-1).

It was discussed earlier that the phase and amplitude of MISOs are better simulated in the presence of the diurnal cycle of the sea surface. Therefore, we further analyze whether the dynamical features necessary for MISO propagation are improved in the presence of diurnal SST. In Fig. 2, the middle panel shows the vertical structure of various parameters around the convection center. The meridional asymmetry and northward shift in these parameters showing boundary layer convergence leading to the convection center are reasonably well simulated by CFSv2 (CTL) simulations. However, a few limitations compared to observation can be noted, such as the axis of maximum vertical velocity, specific humidity, and moist static energy do not show northward tilt at lower levels as observed in reanalysis. Also, the extent of the northward shift of ascending motion and boundary layer convergence is smaller in the CTL simulation than in the reanalysis. From SEN run with the diurnal cycle over oceans, the tilt in maximum ascending motion at the lower level is seen and is better simulated as it shifts around 6° (~2° more than the CTL run) north of the convection center. The divergence plot also shows the intensification of lower-level convergence and upper-level divergence in the SEN run as compared to the CTL run. A clear northward shift of maximum lower-level convergence can also be seen in the SEN run (1.5°), unlike that of the CTL run (0.5°). The north-south extension of moisture availability with a farther northward shift of maximum specific humidity in the SEN run is similar to reanalysis, which was a major limitation in CTL

simulations. The axial tilt in specific humidity is also better represented in SEN. Therefore, the vertical profiles of specific humidity and divergence in CTL and SEN run indicate a stronger anomalous moisture convergence when the diurnal cycle of SST is implemented. Comparing the vertical profiles of vorticity shows that the positive barotropic vorticity is shifted north of the convection center in SEN run compared to the CTL run. Therefore, the presence of a diurnal cycle in SST helped towards a better simulation of dynamical features required for coherent poleward propagation of MISOs. The next section will discuss how both simulations compare the air-sea interaction processes during the MISO life cycle.

3.3 Air-Sea Interaction

The critical role of SST and air-sea interactive fluxes during the coupled evolution and northward propagation of monsoon intra-seasonal oscillations have been extensively studied by researchers in the past (Shinoda et al. 1998; Kemball-Cook and Wang 2001; Sengupta et al. 2001; Fu et al. 2003; Ajayamohan et al. 2008; Li et al. 2018). The studies mentioned above have shown the lead-lag relations between SST, surface net heat flux (Q_{net}), and convective anomalies during different phases of intra-seasonal oscillation over the Indian Ocean, BoB, and AS. To evaluate the role of the diurnal cycle of SST on the northward propagation of MISOs, further analysis of air-sea interaction characteristics is carried out. In Fig.1(a)-(c), the contours represent the filtered SST anomalies during the active spell over central India. Warmer (cooler) SST anomalies before (after) the active phase can be seen in observation and are in line with earlier studies (Fu et al. 2003; Li et al. 2018). At the intra-seasonal scale, Q_{net} drives the intra-seasonal SST changes during the coupled evolution and northward propagation of monsoon intra-seasonal oscillations (Shinoda et al. 1998; Sengupta al. 2001). During monsoon season, over the BoB, variability in latent heat flux and solar radiation dominates towards Q_{net} variability over all other heat fluxes. Fig.1 (d) shows the filtered Q_{net} anomalies as shading and filtered LHF anomalies as contours in reanalysis during the coherent propagation of MISO. The convention used for Q_{net} and LHF is Qnet is positive downward, and LHF is positive upward. Q_{net} anomalies are approximately out of phase with convection, where negative (positive) Q_{net} anomalies cooccur with positive (negative) precipitation anomalies. The net heat flux anomalies are also in quadrature with SST anomalies with positive Q_{net} leading warmer SST anomalies. The latent heat flux varies out of phase with Q_{net}, and negative LHF anomalies are seen before the active spell resulting in warmer SST anomalies. Therefore, during the break spell, Q_{net} increases due to the combined effect of reduced LHF (due to weaker winds) and increased solar radiation. The enhanced heat in the ocean causes the sea surface to warm. Although these warmer SSTs can be a response to the break phase due to clear sky conditions, they can help initiate and propagate active spell (Sengupta et al. 2001; Ajayamohan et al. 2008) by destabilizing the lower atmosphere (Lindzen and Nigam 1987; Roxy and Tanimoto 2007). Fig.1 (g) shows the convergence terms of column integrated moist (colour shading) and MSE (contour) budget equation. The figures show enhanced (positive anomalies) moisture convergence posterior to the warm SST anomalies and during active spells. On the other hand, the recharge of moist static energy through MSE convergence during the preceding break and discharge of moist static energy through MSE divergence can also be noted.

Therefore, during the monsoon break phase, MSE builds up due to enhanced Q_{net} and warming, causing increased boundary layer convergence.

Comparing model simulations (Fig.1) against the observation/reanalysis indicates that the model's lead-lag relation between ocean, atmosphere and air-sea interaction parameters are satisfactorily well represented. But significant differences in the magnitude organization of anomalies can be noted between the two model simulations. The warmer SST anomalies before a stronger active phase are seen (Fig.1 b-c) in the SEN run (~0.3°C) compared to the CTL run (~0.25°C). Also, SST anomalies are cooler in SEN run than CTL run posterior to the active phase. The reason for warmer SSTs before the active spell in SEN run is due to the better representation of rectification of intra-seasonal SSTs (discussed in the following sections) by diurnal warming during the break phase of the monsoon. Rectification is the process of enhancement of intra-seasonal SST variability by diurnal warming and is reported in observational (Mujumdar et al. 2011; Yan et al. 2021) as well as modelling studies (Shinoda 2005; Bernie et al. 2007; Guemas et al. 2011). During the suppressed convection, the surface winds are weak, along with higher solar radiation due to less cloud cover. In these conditions, the weak shear-driven mixing is stabilized by enhanced buoyancy due to the absorption of solar radiation. As a result, the shallow mixed layer rapidly warms up with net heat gain. Therefore, during the suppressed phase, the amplitude of diurnal warming is significantly higher. The enhanced (reduced) diurnal warming during suppressed (active) phase can increase (decrease) the daily mean SST, and therefore it can enhance the magnitude of intra-seasonal SST variability. Hence, with the implementation of diurnal skin temperature parameterization, the intra-seasonal SST variability in SEN run gets amplified compared to the CTL run, which does not have diurnal warm-layer-cool-skin temperature parameterization. The underlying mechanism of warmer SSTs in the presence of diurnal skin temperature schemes is reflected in intra-seasonal anomalies of MLD (figure not shown), Q_{net} (Fig.1 e-f), LHF (Fig.1 e-f) intra-as well. The warmer SST anomalies during the break spell in the SEN run are associated with reduced LHF, enhanced Q_{net}, and shallower MLD anomalies compared to the CTL run. During the active phase, the associated convective downdrafts in the SEN run can cause a drier boundary layer and cooler surface air (Chen and Houze 1997). Hence, it increases the air-sea temperature and humidity difference, enhancing air-sea interactive fluxes. The stronger winds during a convective period can enhance air-sea flux anomalies. As discussed earlier, the surface heat fluxes and SSTs can modulate the boundary layer convergence, atmospheric stability, and atmospheric energy budgets; a similar impact is evident from Fig. (h)-(i) where convergence terms of moisture (shading) and MSE (contours) energy budgets are plotted as Hovmöller diagrams for CTL and SEN simulations respectively. Enhanced moisture and MSE convergence anomalies throughout northward propagation of MISOs in the SEN run are observed compared to the CTL run. These observations are consistent with the rectification of SSTs in SEN run by by diurnal warming, which plays an important role during the life cycle of MISO by modulation of air-sea fluxes, boundary layer convergence, energetics, and convection.

3.4. Rectification

The previous section highlighted the importance of intra-seasonal SST anomalies on the northward propagation of intra-seasonal anomalies. Based on these discussions, the question arises of why the intra-seasonal SST variability is amplified in SEN run with the implementation of the diurnal cycle of the sea surface. Therefore, the present section addresses why and how the diurnal cycle is expected to impact the intra-seasonal SST variability and related surface and atmospheric processes. Earlier studies, (e.g. Kawai and Wada 2007; Brunke et al. 2008; Pradhan et al. 2022) have shown how the parameterization of the diurnal cycle of SST and air-sea interactive fluxes can improve the diurnal variability of ocean-atmosphere parameters, as well as seasonal and interannual variability in coupled model simulations. The scale interaction between SST at diurnal and longer time scales can be quantified in terms of the persistence of diurnal warming, and is evaluated by computing decorrelation time. The decorrelation time is defined (Guemas et al. 2011) as the time (in days) for which the lagged correlation between diurnal warming (DW) and SST remains significant at a critical level (95%) of significance. Therefore, persistence values indicate to what temporal extent diurnal warming can interact with slower scales. Fig. 3 presents the persistence values over the Indian and Pacific Oceans where Indo-Pacific tropical moored buoys are located. In the tropical Indo-Pacific basin, the observed persistence is mostly greater than 15 days and ranges up to 60 days at a few locations. Both the model simulations could reproduce the persistence values greater than 15 days in most of the Indo-Pacific tropical Ocean. Therefore, diurnal warming in observation and model simulations can impact the intra-seasonal and seasonal SST variabilities. However, some differences between observation and model-simulated persistence patterns can be noticed. For example, observed persistence is higher over the central Pacific Ocean and western Pacific warm pool region than the eastern Pacific Ocean. In CTL simulation, the persistence is higher over the central and eastern Pacific oceans. Therefore, the persistence values are underestimated over the central and western Pacific region and overestimated near the eastern Pacific Ocean. The persistence in SEN run is significantly better than CTL run as it is closer to observation in the western Pacific warm pool region and over the eastern and central Pacific oceans. On the other hand, over the Indian Ocean, both CTL and SEN run agree reasonably well with observations. Since, for most of the regions considered in this study, the diurnal warming persists more than 15 days and can impact the intra-seasonal SST variability, therefore further analysis is carried out to quantify the amplitude contribution of diurnal warming to intra-seasonal SST.

The rectification mechanism through which diurnal SSTs can amplify/subdue the intra-seasonal amplitude of SST has been proposed and discussed in various observational and modelling studies (Shinoda and Hendon 1998; Bernie et al. 2005; Mujumdar et al. 2011; Yan et al. 2021). In this study, the amplitude of rectification by diurnal cycle is computed as

$$Rectification = \frac{ISV_{with} - ISV_{without}}{ISV_{with}} \times 100 \qquad (1)$$

$ISV_{without}$ is calculated as the standard deviation of time series of the night time minimum temperature (otherwise know as foundation SST) which is assumed to be independent of diurnal cycle, whereas

ISV_{with} is calculated as the standard deviation of hourly and 3-hourly SST dataset in observation and model respectively. Therefore, ISV_{with} and $ISV_{without}$ are the intraseasonal standard deviations of SST with and without diurnal cycle, respectively. The numerator of Equation-1 is equivalent to intraseasonal standard deviation of diurnal SST and the ratio describes the contribution (in percentage) of diurnal SST to the intraseasonal variability of total SST. The observed and model-simulated amplitude of rectification is shown in Fig 4 at various buoy locations. The observed contribution is found to be positive over the western tropical Pacific Ocean and Indian Ocean and negative over the equatorial eastern Pacific Ocean. These findings agree with the previous study of Yan et al. (2021), with a minor difference in magnitude because of the difference in the analysis period. In the present study, only buoys having continuous high-frequency (hourly) data for at least five years are considered, while Yan et al. (2021) have not considered such criteria. The diurnal SST tends to enhance intra-seasonal SST variability over Indo-Pacific warm pool region, whereas it weakens the intra-seasonal variability over the eastern equatorial Pacific Ocean. Such asymmetric association of diurnal and intra-seasonal SST is due to differential air-sea interactions at the eastern and western Pacific Oceans, as suggested by Yan et al. (2021). Over the western equatorial Pacific, ocean is highly governed by atmospheric processes, whereas over the eastern equatorial Pacific, the atmospheric processes are governed by oceanic processes. In the eastern equatorial Pacific region, the warmer (cooler) SSTs are favorable for enhanced (reduced) convection with stronger (weaker) winds which reduces (enhances) the amplitude of diurnal SST. Therefore, intraseasonal SST and diurnal SST are in opposite phase with each other over the equatorial cold tongue region. On the other hand, over the western equatorial Pacific region, due to enhanced (reduced) convection with stronger (weaker) winds both SST and diurnal SST are reduced (enhanced). Therefore, intraseasonal SST and diurnal SST are in same phase with each other over the western Pacific warm pool region. The comparison of model simulations against the observation indicates that throughout the Indo-Pacific basin, the rectification is weaker, i.e., underestimated in the CTL run. In contrast, the same is improved and closer to observation in the SEN run. The observed amplitude of rectification over the tropical western Pacific region is 8-10%, whereas the same in the CTL run is 2-3%. But in the SEN run, the amplitude of rectification is significantly enhanced and ranges between 3-10%. Also, the CTL simulation shows a weakening of intraseasonal SST variability due to diurnal SST at various locations (between 5°S-0°N and 150°E-170°E) over the western Pacific Ocean which is not realistic. At these locations, CTL run produces negative rectification whereas SEN run produces positive rectification similar to observation. Therefore, the SEN simulation is improved and realistic with the revised flux and skin temperature scheme. Over the northern Indian Ocean also, the amplitude of rectification is enhanced in SEN run compared to the CTL run and is closer to the observed amplitude. Therefore, the more accurate persistence and amplitude of SST rectification seen in the presence of diurnal skin temperature parameterization can eventually lead to a better representation of air-sea interaction and convection during different phases of MISO. The diurnal warm layers over the BoB are strong (Mujumdar et al., 2011) and to study them high frequency observations of ocean state are needed. But continuous high frequency observation through buoy network in Indian ocean is very poor. Hence, a complete picture of rectification throughout the Indian Ocean could not be not be represented in this study.

3.5. Diurnal Sea Surface Warming and its relation to the atmosphere

Bellenger et al. (2010) used 30 days of in situ observations and showed the possible association of diurnal sea surface warming with atmospheric boundary layer and convective processes. Most of their discussion is confined to addressing the diurnal behaviour of convective features in the presence/absence of diurnal warm layers. However, their results (specifically Fig 3 of their study) also showed that subdued convective processes and calm wind conditions accompany diurnal warming events. Strong diurnal warming events are found to be associated with reduced daily mean latent/sensible heat, reduced horizontal wind, reduced downdraft, shallow atmospheric mixed layer, and reduced precipitation. In the current section, analysis is carried out to validate these inferences and to see how these associations are simulated without and with diurnal skin temperature parameterization. Composite analysis of atmospheric fields is carried out by defining strong diurnal warming (SDW) and weak diurnal warming (WDW) events. SDW(WDW) events are determined as the days when the diurnal range of SST (dSST) is greater (less) than 1(-1) standard deviation from its seasonal mean. Fig. 5 shows the composite horizontal wind speed at 10m during SDW and WDW events. From observation, it is evident that during SDW events, the horizontal winds are calmer over the Indo-Pacific Ocean than during WDW events. However, stronger winds along the Somalia jet region region can be seen during strong warming events compared to other regions. On the other hand, relatively weaker winds are seen over the equatorial Indo-Pacific regions compared to other regions during weak warming days. Comparing model simulations against the observation indicates that CTL simulation produces stronger winds over off-equatorial regions during strong warming days compared to observations. On the other hand, the SEN run with diurnal SST parameterization reproduces the wind conditions over the Indo-Pacific basin realistically closer to observation. During WDW events, the model simulations agree with observation except for the underestimation of wind speed over the north-Pacific Ocean in CTL simulations. Similarly, a composite of surface latent heat flux during SDW and WDW days for observation and simulations is plotted in Fig. 7. Observation shows the magnitude of latent heat flux is lower during SWD days than DWD days. This agrees with Bellenger et al. (2010), who have shown reduced daily mean latent heat during strong diurnal warming days. The higher daily mean latent heat flux during WDW days is well reproduced by both the model simulations with overestimation in magnitude in both CTL and SEN. However, during SDW days, the CTL simulations significantly overestimate the latent heat flux compared to observation and SEN simulations. In the CTL run, no clear difference in latent heat fluxes is noticed between SDW and WDW days. The overestimation of latent heat flux during WDW events can also be linked to the unrealistic higher wind speeds simulated by CTL simulations, as discussed in Fig. 5. However, due to the presence of diurnal SST parameterization along with COARE 3.0 flux scheme, the latent heat flux simulation is significantly better in SEN run compared to CTL run specifically during WDW days. Further analysis is carried out to see the impact of diurnal warming on convective processes. The composite of daily mean precipitation is plotted in Fig. 6 during SDW and WDW days for observation and model simulations. Reduced rainfall during SDW events and enhanced rainfall over the tropical Indian Ocean and western and eastern Pacific Ocean during WDW events can be seen from observed rainfall composites. As

suggested by Fairall et al. 1996 (and references therein), diurnal warming is stronger during clear skies and calm wind conditions. In the CTL run, the simulated rainfall over the tropical eastern Pacific and western Pacific warm pool region during SDW days is of higher magnitude and unrealistic. On the other hand, SEN run realistically produced reduced convection over the Indo-Pacific Ocean. The simulated rainfall patterns during WDW events are similar in CTL, and SEN runs with minor underestimation of rainfall magnitude in CTL run over the equatorial Indo-Pacific Ocean.

Chen and Houze (1997) suggested that convective downdrafts can cause a drier boundary layer and cooler surface air. Hence, it increases the air-sea temperature and humidity difference, enhancing air-sea interactive fluxes. The gusty winds during a convective period can also enhance the air-sea fluxes. These convective features are associated with a reduction in daytime warming in SST. The observed winds, precipitation, and latent heat flux, shown in Fig. 5-7, indicated similar inferences where stronger winds, enhanced precipitation, and enhanced latent heat fluxes are found during weak diurnal warming days. Also, the comparison of model simulations confirms that diurnal skin temperature parameterization is important to simulate a realistic association between the diurnal variability of the sea surface and the atmospheric and air-sea interface.

4. Summary And Conclusion

In the present study, analysis was performed to showcase a more realistic simulation of the phase and amplitude of northward propagating MISO by implementing diurnal skin temperature variability in the coupled model. It is shown that through the rectification process, diurnal warming can enhance/subdue the intra-seasonal SST variability depending on the local ocean-atmosphere feedback processes. Over the Indo-Pacific warm pool region, the rectification process enhances the intra-seasonal SST variability, whereas, over the eastern Pacific cold tongue region, the intra-seasonal SST variability is subdued by diurnal SST variability. Due to the implemented skin temperature parameterization through the COARE algorithm, the SEN run could reproduce the amplification of intra-seasonal SSTs over the Indo-Pacific warm pool region by rectification. At the same time, the CTL simulation lacks in simulating the magnitude (also the sign at a few locations) of rectification over the tropical Indo-Pacific basin. Further analysis highlighted that the relation between diurnal warming and wind speed, precipitation, and heat fluxes during Indian summer monsoon season, which was significantly lacking in CTL simulation, has become realistic in SEN simulations. The combined effect of SST rectification and improved warming-wind-precipitation-flux relation can be seen in northward propagation characteristics of monsoon intra-seasonal oscillations. The low wind and high diurnal warming during monsoon breaks produce warmer intra-seasonal SST anomalies with reduced latent heat, enhanced net heat, and shallower MLD. The air-sea interaction acts so that it helps reduce the discharge of moist static energy by latent heat and higher recharge by convergence before the subsequent active phase. Also, diurnal warming helps in stronger moisture convergence during and after the break phase. As a result of these feedback processes, the following active phase of monsoon is significantly stronger in SEN run than in the CTL run. The atmospheric mechanism supporting the northward propagation of MISO is also verified. In SEN simulation, the essential requirements for coherent propagation of MISO are more pronounced than in

CTL simulations. Tilting of maximum vertical velocity, specific humidity, and moist static energy axis around the convection center is better simulated by the coupled model in the presence of the diurnal cycle of SST. The northward shift of vertical velocity, positive barotropic vorticity, specific humidity, geopotential height, and lower-level convergence with respect to the convection center is also better represented in SEN run. Due to the rectified intra-seasonal SST, the enhanced lower-level moisture convergence is evident as stronger anomalies in specific humidity and low-level convergence leading to the convection center in the SEN run. Therefore, diurnal sea surface temperatures can result in stronger coherent northward propagating MISOs through ocean-atmosphere feedback processes. Therefore, diurnal skin temperature variability parameterisation is essential for better prediction of extended, medium, and seasonal prediction systems using coupled models.

Declarations

Funding

The authors declare that no funds, grants, or other support were received during the preparation of this manuscript.

Competing Interests

The authors have no relevant financial or non-financial interests to disclose.

Author Contributions

All authors contributed to the study conception and design. Coupled model experiments and analysis were carried out by Maheswar Pradhan. The first draft of the manuscript was written by Maheswar Pradhan and Dr. Suryachandra A. Rao and Prof. Amitabh Bhattacharya commented on previous versions of the manuscript. All authors read and approved the final manuscript.

Data Availability

The coupled model hindcast datasets generated during and/or analysed during the current study are not publicly available due to its large size but are available from the corresponding author on reasonable request.

References

1. Ajayamohan RS, Rao SA, Yamagata T. 2008. Influence of Indian ocean dipole on poleward propagation of boreal summer intraseasonal oscillations. *Journal of Climate*, 21(21).

https://doi.org/10.1175/2008JCLI1758.1.

2. ALEXANDER G, KESHAVAMURTY RN, DE US, CHELLAPPA R, DAS SK, PILLAI P v. 1978. Fluctuations of monsoon activity. *MAUSAM*, 29(1). https://doi.org/10.54302/mausam.v29i1.2862.
3. Bellenger H, Takayabu YN, Ushiyama T, Yoneyama K. 2010. Role of Diurnal Warm Layers in the Diurnal Cycle of Convection over the Tropical Indian Ocean during MISMO. *Monthly Weather Review*. American Meteorological Society, 138(6): 2426–2433. https://doi.org/10.1175/2010MWR3249.1.
4. Bernie DJ, Guilyardi E, Madec G, Slingo JM, Woolnough SJ. 2007. Impact of resolving the diurnal cycle in an ocean–atmosphere GCM. Part 1: a diurnally forced OGCM. *Climate Dynamics 2007 29:6*. Springer, 29(6): 575–590. https://doi.org/10.1007/S00382-007-0249-6.
5. Bernie DJ, Woolnough SJ, Slingo JM, Guilyardi E. 2005. Modeling diurnal and intraseasonal variability of the ocean mixed layer. *Journal of Climate*. American Meteorological Society, 18(8): 1190–1202. https://doi.org/10.1175/JCLI3319.1.
6. Brunke MA, Zeng X, Misra V, Beljaars A. 2008. Integration of a prognostic sea surface skin temperature scheme into weather and climate models. *Journal of Geophysical Research Atmospheres*. Blackwell Publishing Ltd, 113(21): D21117. https://doi.org/10.1029/2008JD010607.
7. Chen SS, Houze RA. 1997. Diurnal variation and life-cycle of deep convective systems over the tropical pacific warm pool. *Quarterly Journal of the Royal Meteorological Society*. John Wiley & Sons, Ltd, 123(538): 357–388. https://doi.org/10.1002/QJ.49712353806.
8. Clayson CA, Bogdanoff AS. 2013. The Effect of diurnal sea surface temperature warming on climatological air-sea fluxes. *Journal of Climate*, 26(8). https://doi.org/10.1175/JCLI-D-12-00062.1.
9. Curry JA, Bentamy A, Bourassa MA, Bourras D, Bradley EF, Brunke M, Castro S, Chou SH, Clayson CA, Emery WJ, Eymard L, Fairall CW, Kubota M, Lin B, Perrie W, Reeder RA, Renfrew IA, Rossow WB, Schulz J, Smith SR, Webster PJ, Wick GA, Zeng X. 2004. SEAFLUX. *Bulletin of the American Meteorological Society*. American Meteorological Society, 85(3): 409–424. https://doi.org/10.1175/BAMS-85-3-409.
10. Dai A, Trenberth KE. 2004. The Diurnal Cycle and Its Depiction in the Community Climate System Model in: Journal of Climate Volume 17 Issue 5 (2004). *Journal of Cimateimate*, 17(5): 930–951. https://doi.org/https://doi.org/10.1175/1520-0442(2004)017<0930:TDCAID>2.0.CO;2.
11. Dunning CM, Turner AG, Brayshaw DJ. 2015. The impact of monsoon intraseasonal variability on renewable power generation in India. *Environmental Research Letters*, 10(6). https://doi.org/10.1088/1748-9326/10/6/064002.
12. Dutta U, Hazra A, Chaudhari HS, Saha SK, Pokhrel S, Shiu CJ, Chen JP. 2021. Role of Microphysics and Convective Autoconversion for the Better Simulation of Tropical Intraseasonal Oscillations (MISO and MJO). *Journal of Advances in Modeling Earth Systems*, 13(10). https://doi.org/10.1029/2021MS002540.
13. Fairall CW, Bradley EF, Godfrey JS, Wick GA, Edson JB, Young GS. 1996a. Cool-skin and warm-layer effects on sea surface temperature. *Journal of Geophysical Research: Oceans*. John Wiley & Sons, Ltd, 101(C1): 1295–1308. https://doi.org/10.1029/95JC03190.

14. Fairall CW, Bradley EF, Hare JE, Grachev AA, Edson JB. 2003. Bulk parameterization of air-sea fluxes: Updates and verification for the COARE algorithm. *Journal of Climate*, 16(4): 571–591. https://doi.org/10.1175/1520-0442(2003)016<0571:BPOASF>2.0.CO;2.
15. Fairall CW, Bradley EF, Rogers DP, Edson JB, Young GS. 1996b. Bulk parameterization of air-sea fluxes for Tropical Ocean-Global Atmosphere Coupled-Ocean Atmosphere Response Experiment. *Journal of Geophysical Research*, 101(C2): 3747. https://doi.org/10.1029/95JC03205.
16. Fu X, Wang B, Li T, McCreary JP. 2003. Coupling between Northward-propagating, intraseasonal oscillations and sea surface temperature in the Indian Ocean. *Journal of the Atmospheric Sciences*. American Meteorological Society, 60(15): 1733–1753. https://doi.org/10.1175/1520-0469(2003)060<1733:CBNIOA>2.0.CO;2.
17. Gadgil S, Rupa Kumar K. (n.d.). The Asian monsoon — agriculture and economy. *The Asian Monsoon*. Springer Berlin Heidelberg, 651–683.
18. Ganai M, Mukhopadhyay P, Krishna RPM, Abhik S, Halder M. 2019. Revised cloud and convective parameterization in CFSv2 improve the underlying processes for northward propagation of Intraseasonal oscillations as proposed by the observation-based study. *Climate Dynamics*, 53(5–6). https://doi.org/10.1007/s00382-019-04657-9.
19. Goswami BB, Deshpande M, Mukhopadhyay P, Saha SK, Rao SA, Murthugudde R, Goswami BN. 2014. Simulation of monsoon intraseasonal variability in NCEP CFSv2 and its role on systematic bias. *Climate dynamics*. Springer, 43(9–10): 2725–2745.
20. Goswami BN, Ajaya Mohan RS. 2001. Intraseasonal oscillations and interannual variability of the Indian summer monsoon. *Journal of Climate*, 14(6). https://doi.org/10.1175/1520-0442(2001)014<1180:IOAIVO>2.0.CO;2.
21. Goswami BN, Shukla J. 1984. Quasi-periodic oscillations in a symmetric general circulation model. *Journal of the Atmospheric Sciences*, 41(1). https://doi.org/10.1175/1520-0469(1984)041<0020:qpoias>2.0.co;2.
22. Guemas V, Salas-Mélia D, Kageyama M, Giordani H, Voldoire A. 2011. Impact of the Ocean Mixed Layer Diurnal Variations on the Intraseasonal Variability of Sea Surface Temperatures in the Atlantic Ocean. *Journal of Climate*. American Meteorological Society, 24(12): 2889–2914. https://doi.org/10.1175/2010JCLI3660.1.
23. Huffman GJ, Adler RF, Bolvin DT, Nelkin EJ. 2010. The TRMM Multi-Satellite Precipitation Analysis (TMPA). *Satellite Rainfall Applications for Surface Hydrology*. Springer, Dordrecht, 3–22. https://doi.org/10.1007/978-90-481-2915-7_1.
24. Jiang X, Li T, Wang B. 2004. Structures and mechanisms of the northward propagating boreal summer intraseasonal oscillation. *Journal of Climate*, 17(5). https://doi.org/10.1175/1520-0442(2004)017<1022:SAMOTN>2.0.CO;2.
25. Kawai Y, Wada A. 2007. Diurnal sea surface temperature variation and its impact on the atmosphere and ocean: A review. *Journal of Oceanography 2007 63:5*. Springer, 63(5): 721–744. https://doi.org/10.1007/S10872-007-0063-0.

26. Kemball-Cook S, Wang B. 2001. Equatorial waves and air-sea interaction in the boreal summer intraseasonal oscillation. *Journal of Climate*, 14(13). https://doi.org/10.1175/1520-0442(2001)014<2923:EWAASI>2.0.CO;2.
27. Krishnamurti TN, Oosterhof DK, Mehta A v. 1988. Air-sea interaction on the time scale of 30 to 50 days. *Journal of the Atmospheric Sciences*, 45(8). https://doi.org/10.1175/1520-0469(1988)045<1304:AIOTTS>2.0.CO;2.
28. Krishnamurti TN, Subrahmanyam D. 1982. The 30-50 day mode at 850 mb during MONEX. *Journal of the Atmospheric Sciences*, 39(9). https://doi.org/10.1175/1520-0469(1982)039<2088:TDMAMD>2.0.CO;2.
29. Kumar BP, Vialard J, Lengaigne M, Murty VSN, McPhaden MJ. 2011. TropFlux: air-sea fluxes for the global tropical oceans—description and evaluation. *Climate Dynamics 2011 38:7*. Springer, 38(7): 1521–1543. https://doi.org/10.1007/S00382-011-1115-0.
30. Large WG, Yeager SG. 2009. The global climatology of an interannually varying air - Sea flux data set. *Climate Dynamics*, 33(2–3). https://doi.org/10.1007/s00382-008-0441-3.
31. Li Y, Han W, Wang W, Zhang L, Ravichandran M. 2018. The Indian summer monsoon intraseasonal oscillations in CFSv2 forecasts: Biases and importance of improving air-sea interaction processes. *Journal of Climate*, 31(14). https://doi.org/10.1175/JCLI-D-17-0623.1.
32. Lindzen RS, Nigam S. 1987. On the Role of Sea Surface Temperature Gradients in Forcing Low-Level Winds and Convergence in the Tropics. *Journal of the Atmospheric Sciences*, 44(17). https://doi.org/10.1175/1520-0469(1987)044<2418:otross>2.0.co;2.
33. Madden RA, Julian PR. 1971. Detection of a 40–50 Day Oscillation in the Zonal Wind in the Tropical Pacific. *Journal of the Atmospheric Sciences*. American Meteorological Society, 28(5): 702–708. https://doi.org/10.1175/1520-0469(1971)028<0702:doadoi>2.0.co;2.
34. Masson S, Terray P, Madec G, Luo JJ, Yamagata T, Takahashi K. 2012. Impact of intra-daily SST variability on ENSO characteristics in a coupled model. *Climate Dynamics*. Springer, 39(3): 681–707. https://doi.org/10.1007/s00382-011-1247-2.
35. Mujumdar M, Salunke K, Rao SA, Ravichandran M, Goswami BN. 2011. Diurnal cycle induced amplification of sea surface temperature intraseasonal oscillations over the bay of Bengal in summer monsoon season. *IEEE Geoscience and Remote Sensing Letters*, 8(2): 206–210. https://doi.org/10.1109/LGRS.2010.2060183.
36. Pradhan M, Rao SA, Bhattacharya A, Balasubramanian S. 2022. Improvements in Diurnal Cycle and Its Impact on Seasonal Mean by Incorporating COARE Flux Algorithm in CFS. *Frontiers in Climate*. Frontiers Media S.A., 3: 198. https://doi.org/10.3389/FCLIM.2021.792980/BIBTEX.
37. Prasanna V. 2014. Impact of monsoon rainfall on the total foodgrain yield over India. *Journal of Earth System Science*, 123(5). https://doi.org/10.1007/s12040-014-0444-x.
38. Rao SA, Goswami BN, Sahai AK, Rajagopal EN, Mukhopadhyay P, Rajeevan M, Nayak S, Rathore LS, Shenoi SSC, Ramesh KJ, others. 2019. Monsoon Mission: A targeted activity to improve monsoon prediction across scales. *Bulletin of the American Meteorological Society*, 100(12): 2509–2532.

39. Reeves Eyre JEJ, Zeng X, Zhang K. 2021. Ocean Surface Flux Algorithm Effects on Earth System Model Energy and Water Cycles. *Frontiers in Marine Science*. Frontiers, 0: 403. https://doi.org/10.3389/FMARS.2021.642804.
40. Roxy M, Tanimoto Y. 2007. Role of SST over the Indian Ocean in influencing the intraseasonal variability of the Indian summer monsoon. *Journal of the Meteorological Society of Japan*, 85(3). https://doi.org/10.2151/jmsj.85.349.
41. Roxy M, Tanimoto Y, Preethi B, Terray P, Krishnan R. 2013. Intraseasonal SST-precipitation relationship and its spatial variability over the tropical summer monsoon region. *Climate Dynamics*, 41(1). https://doi.org/10.1007/s00382-012-1547-1.
42. Roy A, Murtugudde R, Sahai AK, Narvekar P, Shinde V, Ghosh S. 2022. Water Savings with Irrigation Water Management at Multi-week Lead Time Using Extended Range Predictions. *Climate Services*. Elsevier B.V., 27. https://doi.org/10.1016/J.CLISER.2022.100320.
43. Sabeerali CT, Ramu Dandi A, Dhakate A, Salunke K, Mahapatra S, Rao SA. 2013. Simulation of boreal summer intraseasonal oscillations in the latest CMIP5 coupled GCMs. *Journal of Geophysical Research Atmospheres*, 118(10): 4401–4420. https://doi.org/10.1002/jgrd.50403.
44. Saha S, Moorthi S, Wu X, Wang J, Nadiga S, Tripp P, Behringer D, Hou YT, Chuang HY, Iredell M, Ek M, Meng J, Yang R, Mendez MP, van den Dool H, Zhang Q, Wang W, Chen M, Becker E. 2014. The NCEP climate forecast system version 2. *Journal of Climate*, 27(6): 2185–2208. https://doi.org/10.1175/JCLI-D-12-00823.1.
45. Sengupta D, Goswami BN, Senan R. 2001. Coherent intraseasonal oscillations of ocean and atmosphere during the Asian Summer Monsoon. *Geophysical Research Letters*. John Wiley & Sons, Ltd, 28(21): 4127–4130. https://doi.org/10.1029/2001GL013587.
46. Seo H, Subramanian AC, Miller AJ, Cavanaugh NR. 2014. Coupled impacts of the diurnal cycle of sea surface temperature on the Madden-Julian oscillation. *Journal of Climate*, 27(22). https://doi.org/10.1175/JCLI-D-14-00141.1.
47. Seo KH, Schemm JKE, Wang W, Kumar A. 2007. The boreal summer intraseasonal oscillation simulated in the NCEP climate forecast system: The effect of sea surface temperature. *Monthly Weather Review*, 135(5). https://doi.org/10.1175/MWR3369.1.
48. Sharmila S, Pillai PA, Joseph S, Roxy M, Krishna RPM, Chattopadhyay R, Abhilash S, Sahai AK, Goswami BN. 2013. Role of ocean-atmosphere interaction on northward propagation of Indian summer monsoon intra-seasonal oscillations (MISO). *Climate Dynamics*, 41(5–6). https://doi.org/10.1007/s00382-013-1854-1.
49. Shinoda T. 2005. Impact of the Diurnal Cycle of Solar Radiation on Intraseasonal SST Variability in the Western Equatorial Pacific. *Journal of Climate*. American Meteorological Society, 18(14): 2628–2636. https://doi.org/10.1175/JCLI3432.1.
50. Shinoda T, Hendon HH. 1998. *Mixed Layer Modeling of Intraseasonal Variability in the Tropical Western Pacific and Indian Oceans*. .

51. Shinoda T, Hendon HH, Glick J. 1998. Intraseasonal Variability of Surface Fluxes and Sea Surface Temperature in the Tropical Western Pacific and Indian Oceans. *Journal of Climate*. American Meteorological Society, 11(7): 1685–1702. https://doi.org/10.1175/1520-0442(1998)011.
52. Sikka DR, Gadgil S. 1980. On the Maximum Cloud Zone and the ITCZ over Indian, Longitudes during the Southwest Monsoon. *Monthly Weather Review*, 1840–1853.
53. Slingo J, Inness P, Neale R, Woolnough S, Yang G. 2003. Scale interactions on diurnal toseasonal timescales and their relevanceto model systematic errors. *Annals of Geophysics*. Instituto Nazionale di Geofisica e Vulcanologia, INGV, 46(1). https://doi.org/10.4401/ag-3383.
54. Vecchi GA, Harrison DE. 2002. Monsoon breaks and subseasonal sea surface temperature variability in the Bay of Bengal. *Journal of Climate*, 15(12). https://doi.org/10.1175/1520-0442(2002)015<1485:MBASSS>2.0.CO;2.
55. Wang B, Xie X. 1997. A Model for the boreal summer intraseasonal oscillation. *Journal of the Atmospheric Sciences*, 54(1). https://doi.org/10.1175/1520-0469(1997)054<0072:AMFTBS>2.0.CO;2.
56. Webster PJ. 1983. Mechanisms of Monsoon Low-Frequency Variability: Surface Hydrological Effects. *Journal of the Atmospheric Sciences*, 2110–2124.
57. Webster PJ, Magaña VO, Palmer TN, Shukla J, Tomas RA, Yanai M, Yasunari T. 1998. Monsoons: processes, predictability, and the prospects for prediction. *Journal of Geophysical Research: Oceans*. Blackwell Publishing Ltd, 103(C7): 14451–14510. https://doi.org/10.1029/97jc02719.
58. Wu MLC, Schubert S, Kang IS, Waliser D. 2002. Forced and free intraseasonal variability over the South Asian monsoon region simulated by 10 AGCMs. *Journal of Climate*, 15(20). https://doi.org/10.1175/1520-0442(2002)015<2862:FAFIVO>2.0.CO;2.
59. Yan Y, Zhang L, Yu Y, Chen C, Xi J, Chai F. 2021. Rectification of the Intraseasonal SST Variability by the Diurnal Cycle of SST Revealed by the Global Tropical Moored Buoy Array. *Geophysical Research Letters*. John Wiley & Sons, Ltd, 48(1): e2020GL090913. https://doi.org/10.1029/2020GL090913.
60. Yasunari T. 1979. Cloudiness Fluctuations Associated with the Northern Hemisphere Summer Monsoon. *Journal of the Meteorological Society of Japan. Ser. II*, 57(3). https://doi.org/10.2151/jmsj1965.57.3_227.
61. Yasunari T. 1980. A Quasi-Stationary Appearance of 30 to 40 Day Period in the Cloudiness Fluctuations during the Summer Monsoon over India. *Journal of the Meteorological Society of Japan. Ser. II*. Meteorological Society of Japan, 58(3): 225–229. https://doi.org/10.2151/JMSJ1965.58.3_225.
62. Yu L, Jin X, Weller R. 2008. Multidecade Global Flux Datasets from the Objectively Analyzed Air-sea Fluxes (OAFlux) Project: Latent and Sensible Heat Fluxes, Ocean Evaporation, and Related Surface Meteorological Variables. *OAFlux Project Technical Report*, OA-2008-01(, 74).

Figures

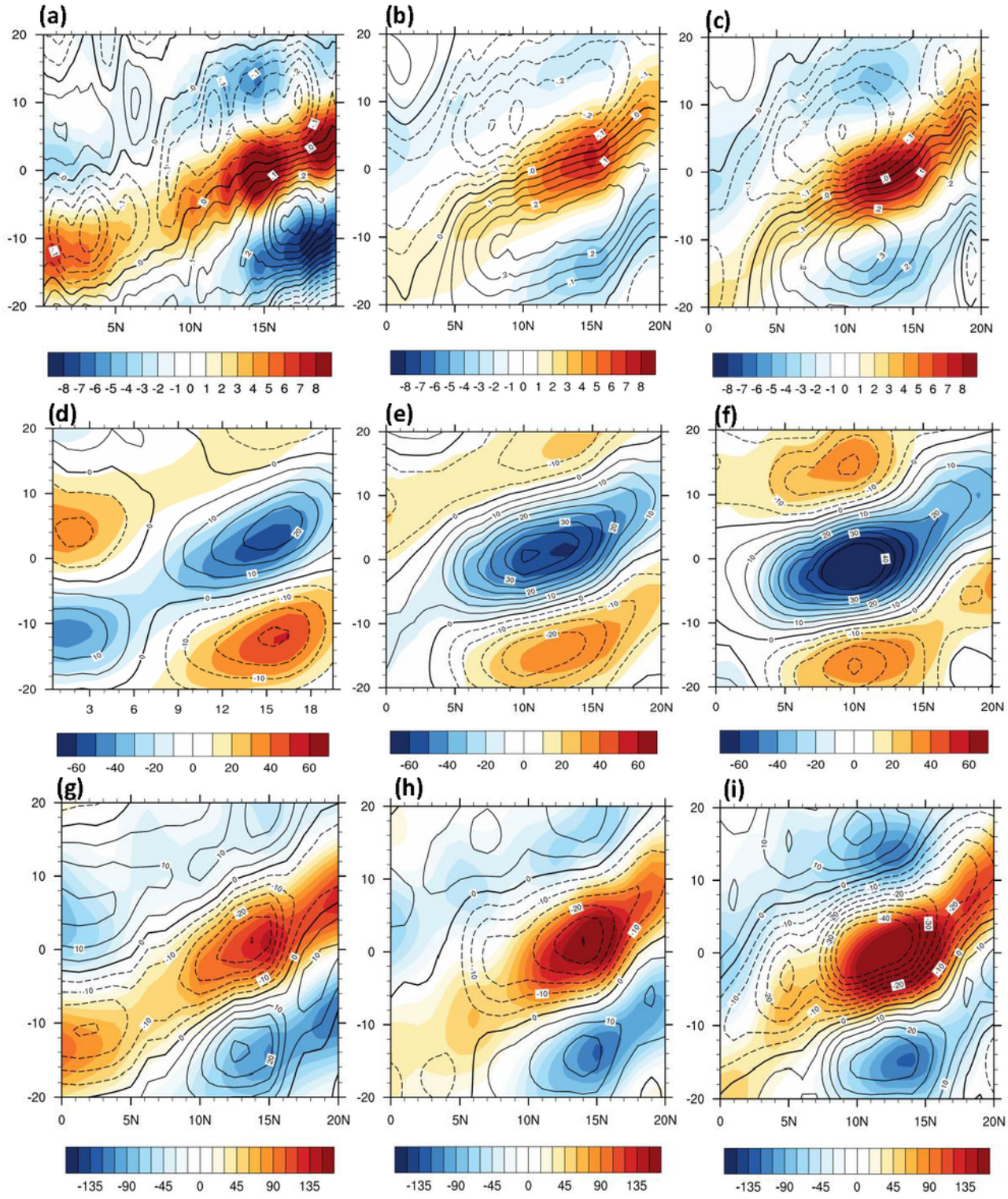

Figure 1

Hovmöller diagrams for filtered rainfall anomalies (mm/day; coloured shading) and SST anomalies (contours) in (a) Observation, (b) CTL run, and (c) SEN run over BoB during active phase of monsoon. (d)-(f) and (g)-(i) same as (a)-(c) but Q_{net} (W/m^2; shading) and latent heat (W/m^2; contour) in (d)-(e) and convergence terms of moisture (W/m^2; shading) and MSE budget (W/m^2; contour) in (g)(i). Horizontal

axis represents the latitude and Vertical axis represents the number of days prior (negative) and after (positive) the peak of break phase over central India (CI).

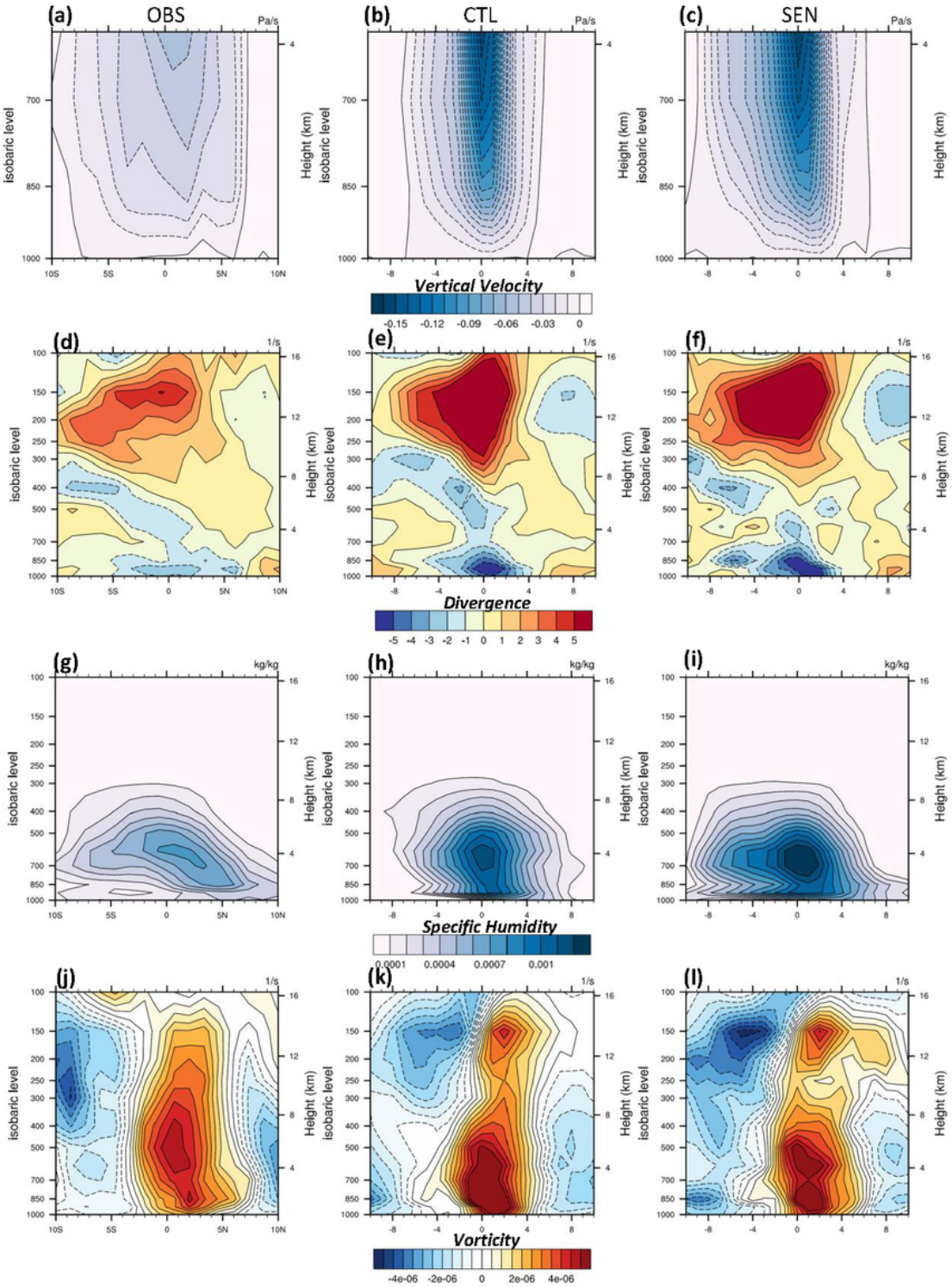

Figure 2

Meridional Vertical Structure of northward propagating MISOs in observation: (a) vertical velocity (Pa s^{-1}), (d) divergence (s^{-1}), (g) specific humidity (kg kg^{-1}), and (j) vorticity (s^{-1}). Horizontal axis represents the

meridional distance (°latitude) from the convection center. The positive (negative) value implies north (south) of convection center. Vertical axis is the altitude (hPa or km). (b), (e), (h), (k) and (c), (f), (i), (l) are same as (a), (d), (g), (j) but for CTL and SEN simulations, respectively.

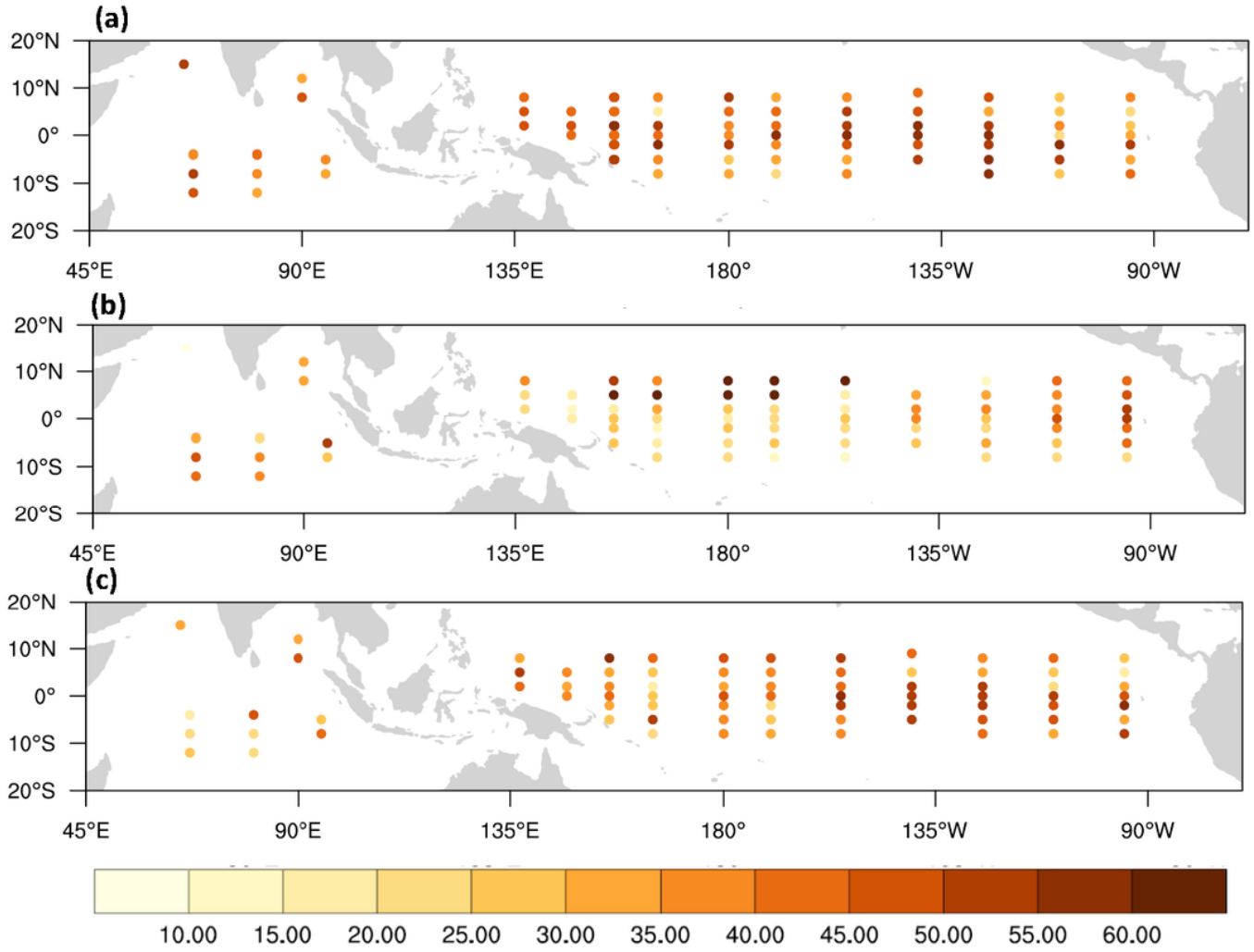

Figure 3

Persistence of dSST (in days) in (a) observation, (b) CTL simulation and (c) SEN simulation respectively.

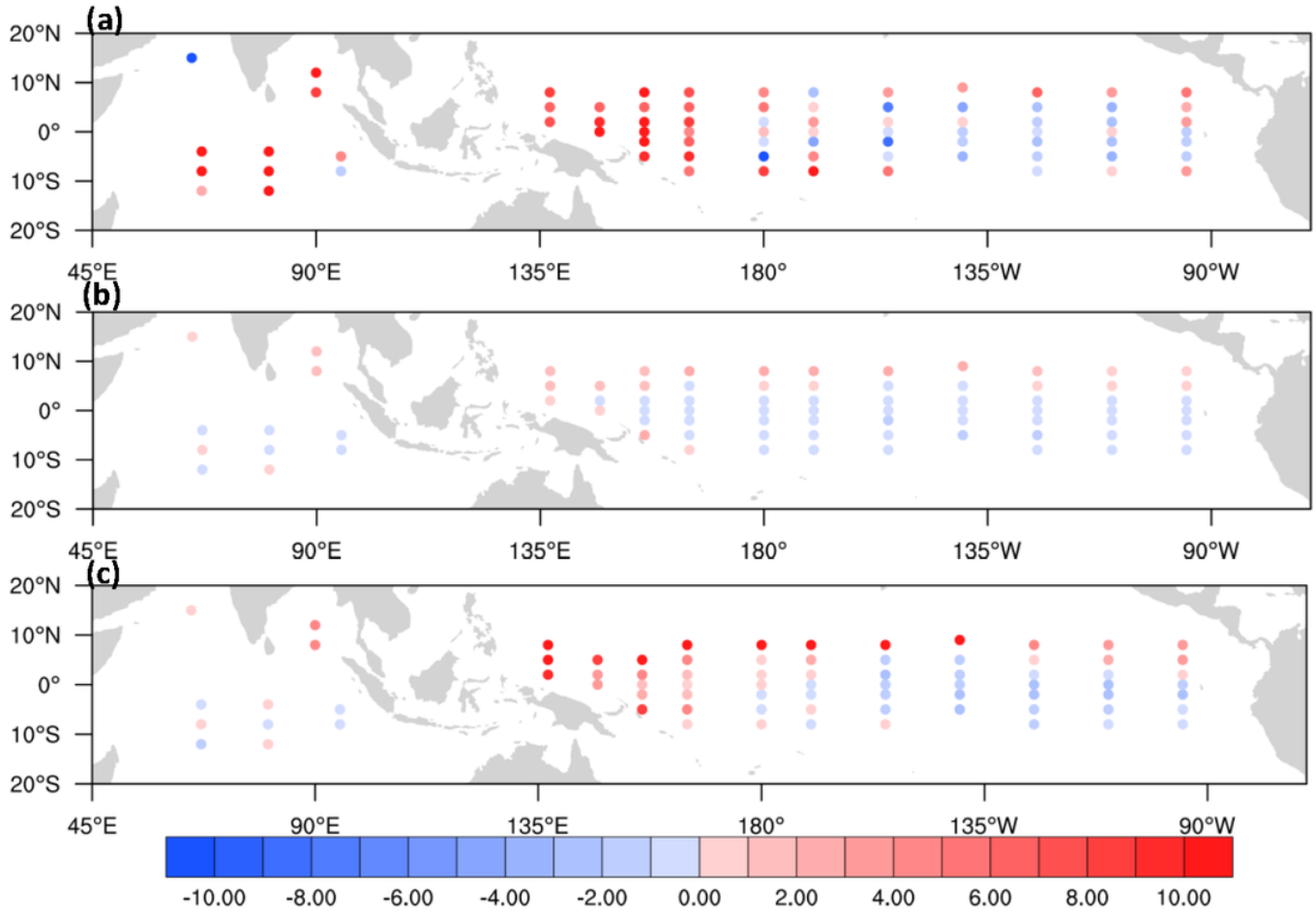

Figure 4

Ratio (in percentage) of intra-seasonal STD of dSST to intra-seasonal (20-100 day filtered during JJAS) STD of SST in (a) observation, (b) CTL simulation, and (c) SEN simulation.

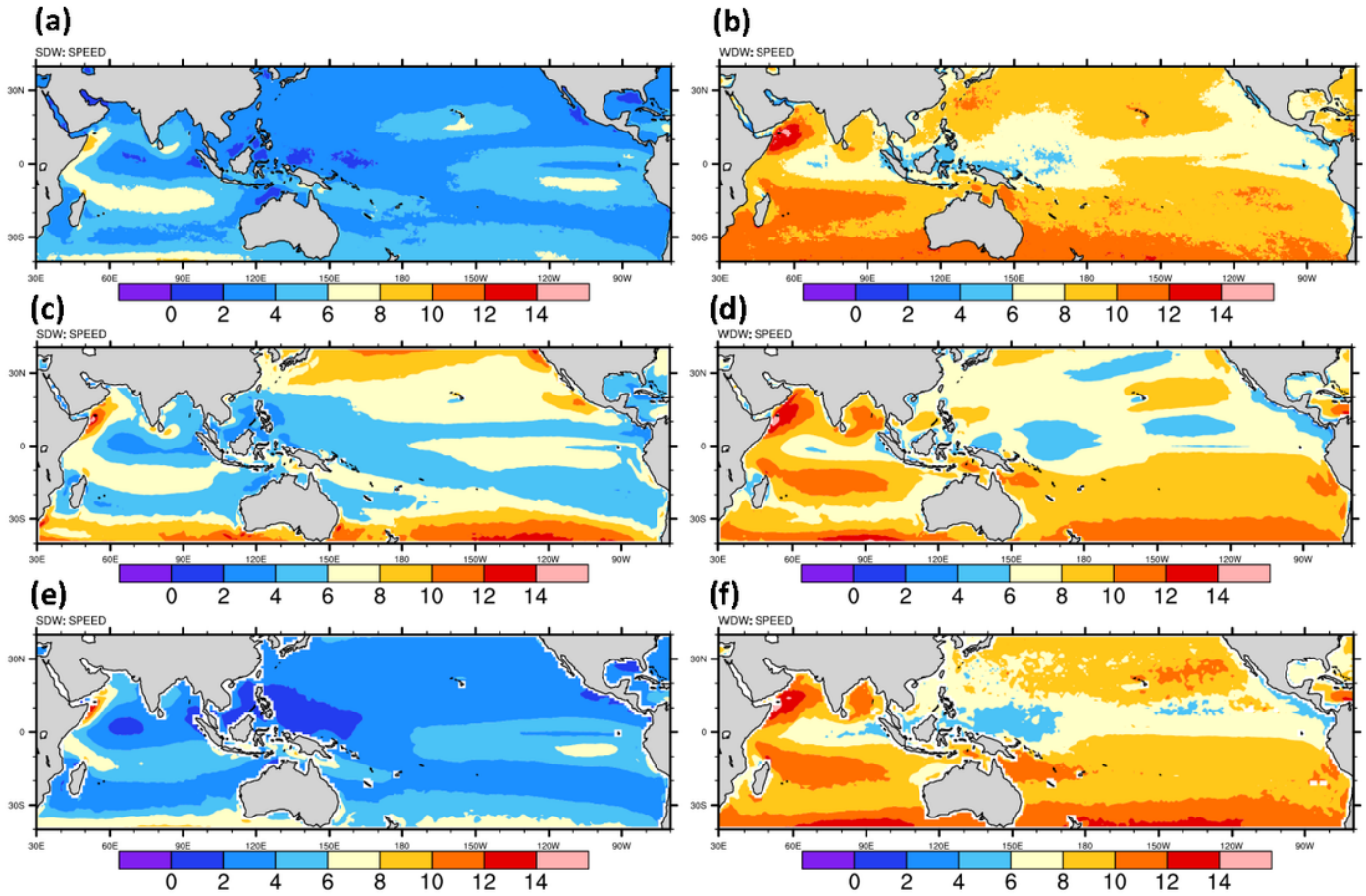

Figure 5

Composite of observed 10m horizontal wind speed (m/s) during (a) Strong Diurnal Warming (SDW) events, and (b) Weak Diurnal Warming (WDW) events. (c), (d) and (e), (f) are same as (a), (b) but for CTL and SEN simulations respectively.

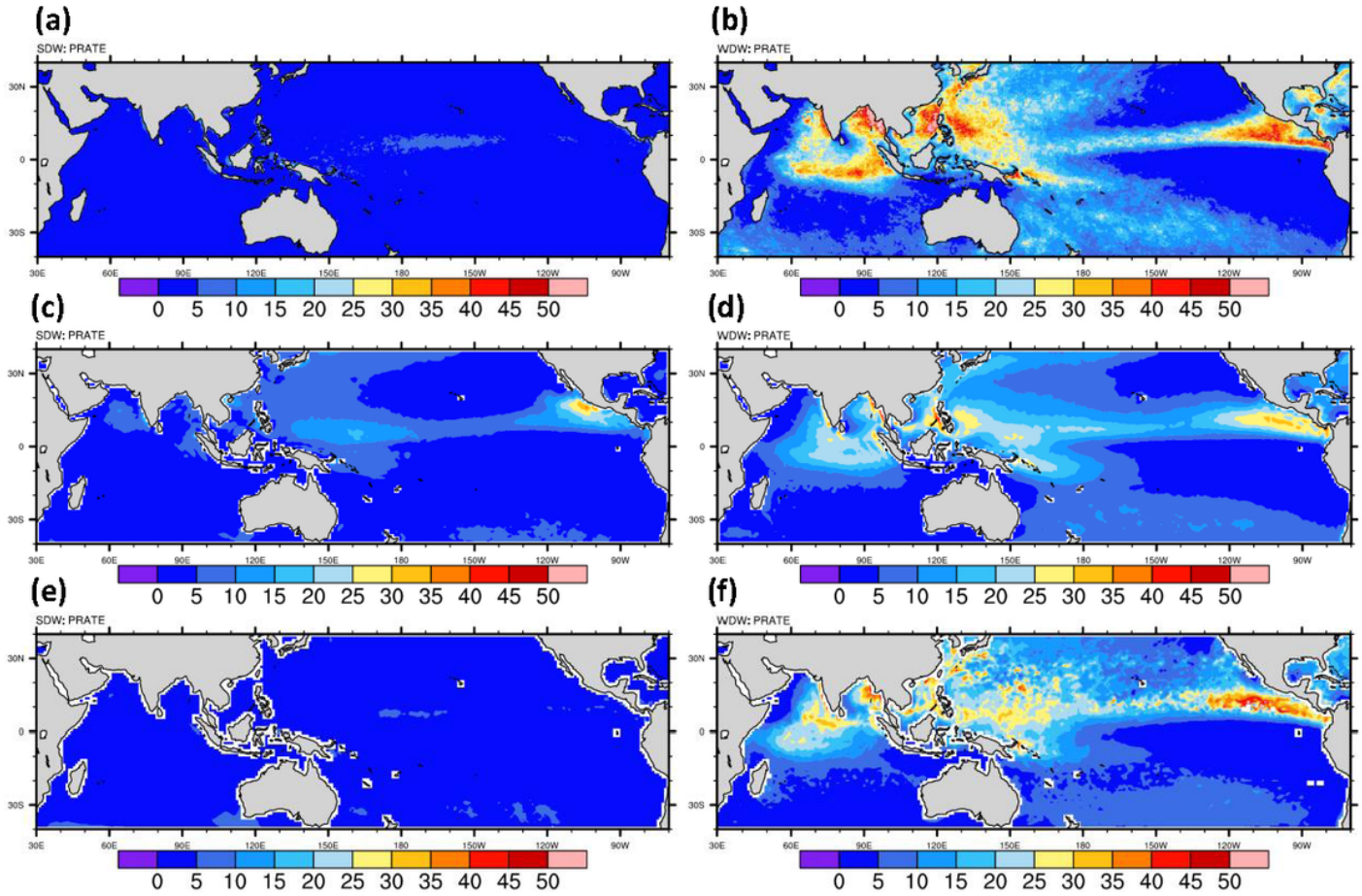

Figure 6

Composite of observed precipitation rate (mm/day) during (a) Strong Diurnal Warming (SDW) events, and (b) Weak Diurnal Warming (WDW) events. (c), (d) and (e), (f) are same as (a), (b) but for CTL and SEN simulations respectively.

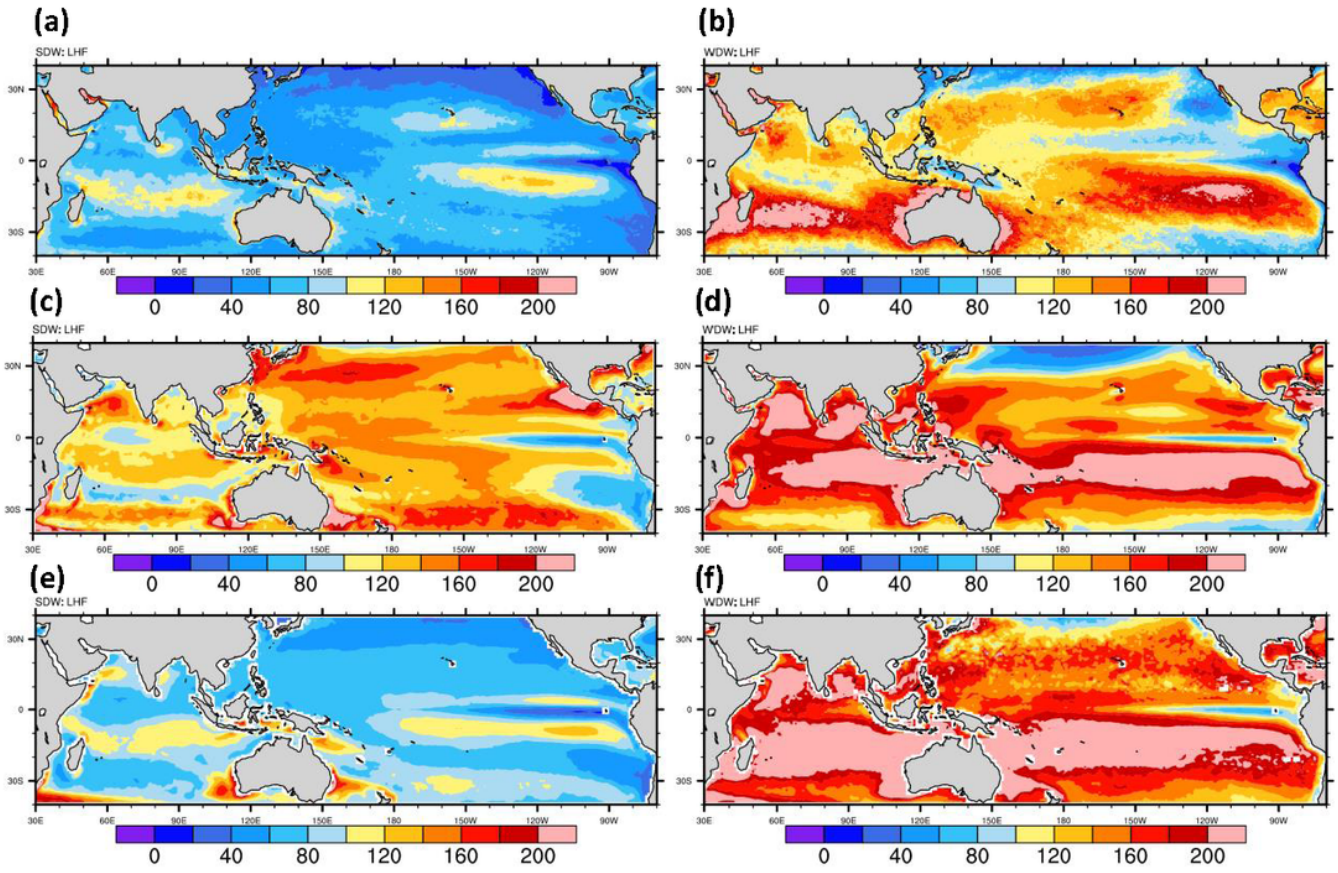

Figure 7

Composite of observed Latent Heat Flux (W/m^2) during (a) Strong Diurnal Warming (SDW) events, and (b) Weak Diurnal Warming (WDW) events. (c), (d) and (e), (f) are same as (a), (b) but for CTL and SEN simulations respectively.

Supplementary Files

This is a list of supplementary files associated with this preprint. Click to download.

- Supplementary1.pdf